Publ. Astron. Soc. Japan 35, 447–453 (1983)

10-GHz Observations of the Supernova Remnant G109.1−1.0 Containing an X-Ray Pulsar

Yoshiaki SOFUE, Fumio TAKAHARA, and Hisashi HIRABAYASHI

Nobeyama Radio Observatory, Minamimaki-mura, Minamisaku-gun, Nagano 384-13*

(Received 1983 March 9; accepted 1983 May 10)

Abstract

The recently discovered supernova remnant G109.1−1.0 which contains an X-ray pulsar was mapped in the radio continuum emission at 10 GHz using the 45-m telescope at the Nobeyama Radio Observatory. A semicircular shell structure is found in global coincidence with an X-ray diffuse structure. No radio enhancement was found at the position of the X-ray pulsar. Instead, a slightly extended radio source is found at the center of the shell, 3′ apart from the X-ray pulsar. An arc-shaped radio ridge extends from the center towards the southern ridge of the shell. The radio spectrum is steep ($\alpha \sim -0.5$ to -0.7) inside the SNR, while it becomes slightly flatter ($\alpha \sim -0.4$) towards the edge. From the surface brightness–diameter relation we estimate its diameter as about 36 pc, the distance as 4.1 kpc, the age as 1.5×10^4 yr, and the expansion velocity as 500 km s^{-1}.

Key words: Radio emission; Supernova remnants; X-ray pulsars.

1. Introduction

The unusual supernova remnant (SNR) G109.1−1.0 having a semicircular X-ray shell of 36′ diameter has been noticed by its central X-ray pulsar with a period of 3.5 s and a jet-like feature emerging from the pulsar (Gregory and Fahlman 1980, 1981; Fahlman and Gregory 1981). The existence of an X-ray pulsar may indicate the existence of a binary system. Studies of this SNR may throw light on the properties of supernova explosion in binary systems.

The SNR has been independently discovered in radio observations at 610 MHz by Hughes et al. (1981). A 2.7-GHz radio continuum map with a resolution of 4′.4 obtained by Downes (1983) shows a semicircular shell structure in global coincidence with the X-ray image. Some optical filaments are found on the shell (Hughes et al. 1981). Because the SNR is near the strong radio source Cas A, not so many good radio observations have been made as yet.

In the present paper we present a map of 10-GHz radio continuum emission of G109.1−1.0 obtained with the 45-m telescope at the Nobeyama Radio Observatory (NRO). We determine the spectral index over the SNR by comparing it with the 2.7-GHz

* Nobeyama Radio Observatory, a branch of the Tokyo Astronomical Observatory, University of Tokyo, is a facility open for general use by researchers in the field of astronomy and astrophysics.

map of Downes (1983). We derive some physical parameters of the SNR on the basis of the present data and discuss the nature of this SNR.

2. Observations

The observations were made on December 14, 1982 using the 45-m telescope. The HPBW of the antenna was $2'.70 \pm 0'.03$ at the center frequency of 10.2 GHz. The bandwidth was 500 MHz. We used a cooled parametric amplifier combined with a Dicke-switching system referencing a cooled dummy load at 20-K stage. The system noise temperature was ~ 100 K. We used a circularly polarized feed system and detected one polarization component. The total intensity was obtained by assuming that circular polarization in the SNR and calibration sources is negligible. The flux density was calibrated using the radio sources 3C161 (3.3 Jy at 10.2 GHz), 3C147 (4.2 Jy), and NGC 7027 (6.5 Jy), whose fluxes were obtained by interpolation of the fluxes given by Baars et al. (1977). The aperture efficiency of the antenna was approximately 60%, and the conversion factor between brightness temperature on the sky and equivalent flux density per beam was $T_b/S = 0.47 \pm 0.05$ K Jy^{-1}. The error in the flux and brightness determination is about $\pm 10\%$, which arises mainly in the process of the calibration.

We mapped a squared area of $48' \times 48'$ centered on R.A. $= 22^h58^m50^s$, Decl. $= 58°36'00''$ (1950). The area was scanned in the right ascension and declination directions at an interval of $1'.2$ and at a speed of $48'$ per 50 s. Assuming flat background emission, we removed it by adjusting two edges of each scan to the zero level of the map. Five maps were obtained, three maps by the declination scan and two by the right ascension scan. The observing time was 40 min per one map, and in total 3.3 hr. Small areas surrounding the calibration sources were mapped for the flux and position calibrations. The position accuracy was better than $0'.3$. The five maps were added to get a final map, on which the rms noise is approximately 3 mK in brightness temperature.

The data reduction was made using a radio astronomical reduction system at the NRO, a part of which contains the NOD2 reduction package described by Haslam (1974). Scanning effects, which are mainly caused by weather conditions, were removed by applying the "pressing method" developed by Sofue and Reich (1979). The computations were carried out on a FACOM M200 and M180IIAD at NRO.

3. Results

The resulting map of the distribution of total intensity at 10 GHz of G109.1−1.0 is shown in figure 1 in the form of a contour map. The contour interval is 5.51 mK in brightness temperature or 11.7 mJy per beam, and the unit of the numbers on the contours is 1.10 mK. Below we describe some features seen from the map.

(*i*) *A compact source, S152*: A strong point-like source appearing near the western rim of the map at R.A. $= 22^h56^m33^s$, Decl. $= 58°30'44''$ is an H II region, S152. Another H II region, S153, is located near S152, $5'$ to the SE. The total flux densities of S152 and S153 are 1.1 ± 0.1 Jy and ~ 0.12 Jy, respectively. Gregory and Fahlman (1980) suggest a relationship between G109.1−1.0 and the H II regions because of the agreement of their distances. Our distance estimate of 4.1 kpc [see (iv)] is also in agreement with the distances to S152 (3.6 kpc) and S153 (4 kpc) estimated by Crampton et al. (1978). However, a glance at figure 1 suggests neither positive nor negative evidence for the relationship.

(*ii*) *Extended features*: The map shows a semicircular shell structure in the eastern

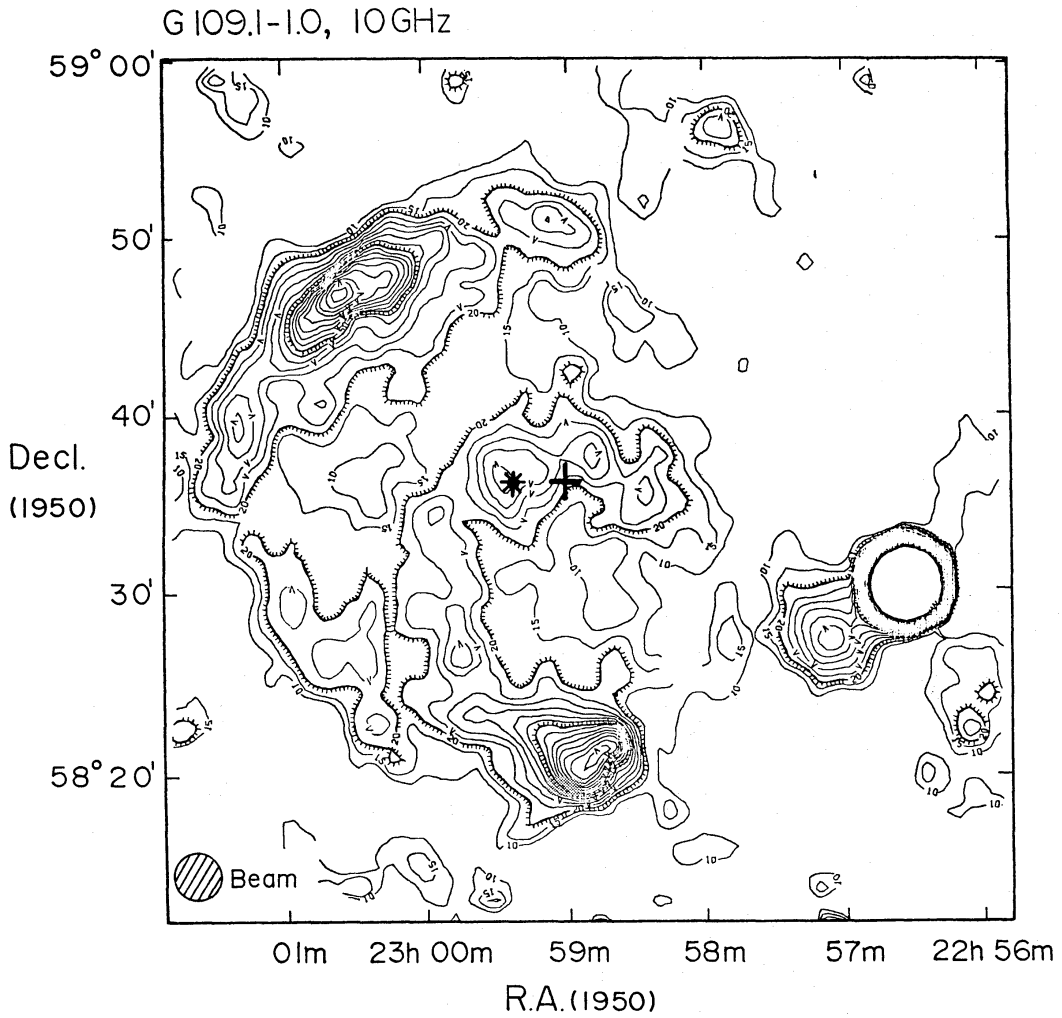

Fig. 1. A total intensity map of the SNR G109.1−1.0 at 10 GHz. The surface brightness temperature is displayed in the form of a contour map. The contour interval is 5.51 mK and the unit of the numbers on the contours is 1.1 mK. The HPBW of the telescope (2.′7) is indicated in the lower left corner. The asterisk is the geometrical center of the shell and the cross is the position of the X-ray pulsar 1E2259+586. A strong point source to the west is the H II region S152 with flux density of 1.1±0.1 Jy.

half. The 10-GHz radio shell is in good positional coincidence with the X-ray shell. The cross in the figure shows the position of the X-ray pulsar 1E2259+586 [R.A.=$22^h59^m03^s.4$, Decl.=58°36′38″ (1950): Fahlman and Gregory (1981)]. The semicircular radio shell is centered on a slightly extended radio source with a flux density of ∼0.3 Jy at R.A.= $22^h59^m30^s$, Decl.=58°35′. The central radio source is 3.′3 away from the X-ray pulsar. We see no significant radio enhancement towards the X-ray pulsar.

An arc-shaped spiral ridge extends from the central source towards the SE and reaches the southern ridge of the shell around its brightest part. A counter extension of the ridge runs from the central source towards the west, passing through the X-ray pulsar position.

A comparison with the X-ray image of G109.1−1.0 of Gregory and Fahlman (1980) shows a global agreement in the shell structure. However, the X-ray jet-like feature is not associated with the radio enhancement. The radio ridge extending from the central

region coincides rather with the X-ray quiet region. The brightest part of the radio shell coincides with the relatively weak X-ray ridge. On the other hand the brightest X-ray ridge in the north is rather less bright in the radio emission. Thus, in spite of the global coincidence, there seems to exist a local anticorrelation between the radio and X-ray brightness.

The 2.7-GHz map of Downes (1983) shows a good agreement with the present 10-GHz map, emphasizing a semicircular shell structure. However, the 2.7-GHz map does not show finer structures as found on the present 10-GHz map because of the wider beam width (4′.4).

(*iii*) *Flux density and spectrum*: Total flux density of G109.1−1.0 at 10.2 GHz was determined to be $S=7.0\pm0.7$ Jy. The flux is compared to the 2.7-GHz flux of $13.0\pm$ 1.5 Jy (Downes 1983). Table 1 lists flux densities of G109.1−1.0 between 408 MHz and 10 GHz from the literature. In figure 2 we plot the fluxes against frequency. The flux distribution is well fitted by a power-law spectrum of index $\alpha=-0.57\pm0.05$ as indicated by the straight line. In the table and figure we have ignored those data obtained earlier than 1965 which might be less reliable compared to those listed here.

The 10-GHz map was smoothed to a HPBW of 4′.4 by a Gaussian beam, and was compared with the 2.7-GHz map of Downes (1983) to get a spectral index distribution. The index was calculated for regions where the brightness in each map exceeds 10σ, where σ

Table 1. Total flux densities of G109.1−1.0.

Frequency (GHz)	Flux density (Jy)	Telescope	HPBW	Reference*
0.408	37.2±7	Bologna interferometer	4′.2×114′	(1)
1.7	25 ±4	Dwingeloo 25 m	24′	(2)
2.7	13 ±1.5	Bonn 100 m	4′.4	(3)
10.2	7.0±0.7	NRO 45 m	2′.7	(4)

* (1) Felli et al. (1977); (2) Hughes et al. (1981); (3) Downes (1983); (4) Present work.

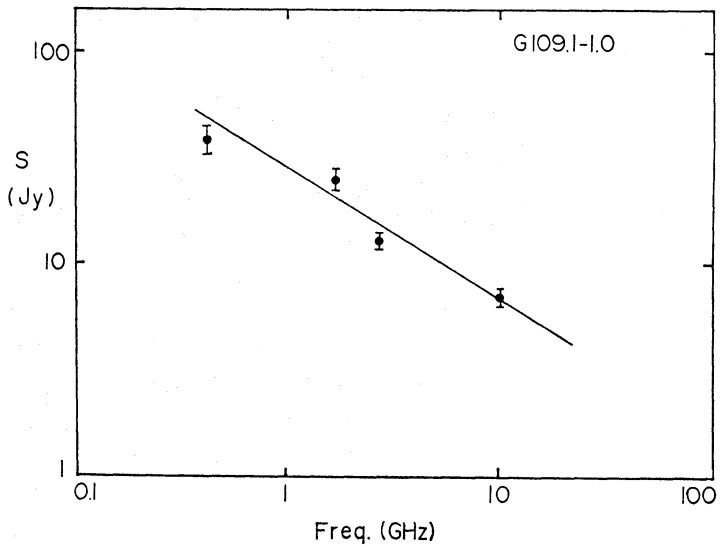

Fig. 2. Total flux densities of G109.1−1.0 plotted against frequency. The data are from table 1. The flux distribution is well fitted with a power-law a spectrum of index $\alpha=-0.57\pm0.05$, which is shown with the straight line.

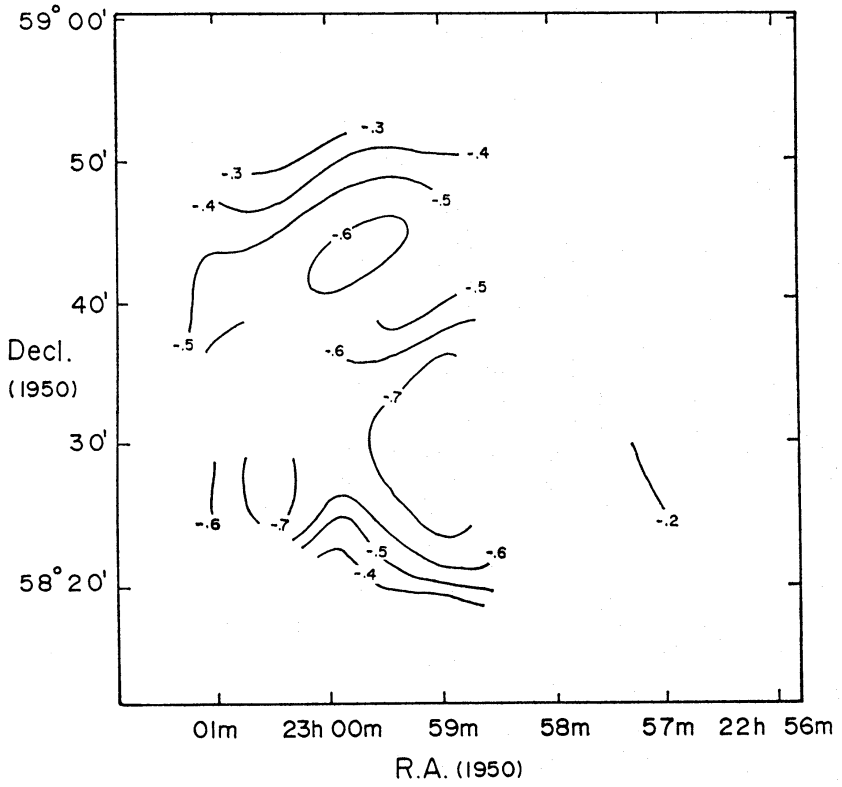

Fig. 3. Distribution of spectral index α of surface brightness between 2.7 and 10 GHz [$\sum$(10 GHz)/$\sum$(2.7 GHz)=(10 GHz/2.7 GHz)$^{\alpha}$].

is the rms noise in the map. Figure 3 shows a map of spectral index α ($\sum \propto \nu^{\alpha}$ with $\sum$ the surface brightness). The spectrum is generally steep in the inner region, while it becomes slightly flatter towards the shell. We note that the spectra of S152 and S153 are as flat as $\alpha \gtrsim -0.2$, consistent with the thermal nature of these H II regions.

(*iv*) *Diameter and distance*: The geometrical center of the shell at 10 GHz, when it is fitted with a circle, is at R.A.=$22^{h}59^{m}21^{s}$, Decl.=58°36′22″ (1950). The diameter of shell is $29'.8 \pm 1'$. The surface brightness averaged over the circle is calculated to be $\sum(10\ \mathrm{GHz}) = 1.2 \times 10^{-21}\ \mathrm{W\ m^{-2}\ Hz^{-1}\ sr^{-1}}$. If we take the spectral index of −0.57, we obtain the surface brightness at 1 GHz as $4.5 \times 10^{-21}\ \mathrm{W\ m^{-2}\ Hz^{-1}\ sr^{-1}}$. Applying a $\sum$–D (surface brightness–diameter) relation for normal SNRs given by Milne (1979),

$$D(\mathrm{pc}) = 4.12 \times 10^{-4} \sum(1\ \mathrm{GHz})^{-0.25} (\mathrm{W\ m^{-2}\ Hz^{-1}\ sr^{-1}}) \exp\left[-|z(\mathrm{pc})|/214\mathrm{pc}\right],$$

we obtain the linear diameter as $D=36$ pc. The corresponding distance and height from the galactic plane are $d=4.1$ kpc and $z=-75$ pc, respectively. Table 2 summarizes the derived parameters.

(*v*) *Age and expansion velocity*: The radius R and expansion velocity v of an SNR shell is related to its initial explosion energy E, the age t, and the ambient gas density ρ through (Sedov 1959)

$$E = \frac{1}{2} \rho R^{5} t^{-2}$$

and

$$v = \frac{2}{5} \frac{R}{t}.$$

Table 2. Derived parameters for G109.1−1.0.

Center position	R.A.(1950)=22h 59m 21s
	Decl.(1950)=58°36′22″
	l=109°.13
	b=−1°.05
Angular diameter	θ=29′.8±1′
Total flux density at 10 GHz	S(10 GHz)=7.0±0.7 Jy
Spectral index (0.6–10 GHz)	α=−0.57±0.05
Surface brightness at 10 GHz	Σ(10 GHz)=1.2×10^{-21} W m^{-2} Hz^{-1} sr^{-1}
Surface brightness at 1 GHz (α=−0.57 is assumed)	Σ(1 GHz)=4.5×10^{-21} W m^{-2} Hz^{-1} sr^{-1}
Diameter*	D=36 pc
Distance	d=4.1 kpc
Height from the galactic plane	z=−75 pc
Expansion velocity†	v=470 km s^{-1}
Age	t=1.5×10^4 yr

* The surface brightness–diameter relation by Milne (1979) is used.

† Explosion energy of E=10^{51} erg and ambient gas density of 0.5 atoms cm^{-3} are assumed.

If the ambient density is of the order of 0.5 atoms cm^{-3} at z=−75 pc and the explosion energy is $E\approx10^{51}$ erg, which is typical of type II SNRs usually associated with a shocked shell, we estimate the age of the shell to be $t\approx1.5\times10^4$ yr and the expansion velocity $v\approx$ 470 km s^{-1}. This age is consistent with that estimated by Gregory and Fahlman (1980) from the X-ray luminosity.

4. Summary and Discussion

Our observational results may be summarized as follows:

(i) A 10-GHz map of G109.1−1.0 reveals a semicircular shell structure, resembling the X-ray image at 0.1–4 keV. However, the jet-like feature in the X-ray is not found in the 10-GHz radio map.

(ii) A slightly extended radio source of ∼0.3 Jy is found at the center of the shell. An arc-shaped radio ridge emerges from the source towards the south and merges with the shell in its brightest part.

(iii) The X-ray pulsar 1E2259+586 is located 3′ away from the central radio source towards the west, i.e., to the direction opposite to the semicircular shell. No radio enhancement is found at the pulsar position.

(iv) The spectral index between 2.7 and 10 GHz is steep in the inner region of G109.1−1.0, while it becomes slightly flatter in the outer region towards the edge.

(v) A surface brightness–diameter relation leads to the diameter and distance of G109.1−1.0 as 36 pc and 4.1 kpc, respectively. The age and expansion velocity are 1.5× 10^4 yr and 470 km s^{-1}.

G109.1−1.0 is one of the supernova remnants which contain a compact X-ray source in the central region. The peculiarity of this object is, however, that the X-ray source may possibly be an accretion-powered X-ray pulsar (Fahlman and Gregory 1981; Fahlman et al. 1982). Also peculiar is that the X-ray pulsar seems to eject an X-ray jet towards the semicircular shell. In this respect it resembles SS433 in the SNR W50, although no X-ray pulsation has been found for SS433. It is puzzling that the X-ray jet turns to a different direction from that of the radio arc found in figure 1, and that no radio and X-ray

features are seen in the western half.

The X-ray pulsar is located eccentric to the radio shell, 3′ (3 pc) away from the center to the opposite direction to the shell; this suggests that the X-ray pulsar is running away at a velocity of about 200 km s^{-1} (projected on the sky). This velocity is of the order of an orbital velocity of close binary systems. A binary system may get a proper motion comparable to the orbital motion, if the more massive component explodes as a supernova but the stellar remnant (neutron star) can still remain bound to the system.

References

Baars, J. W. M., Genzel, R., Pauliny-Toth, I. I. K., and Witzel, A. 1977, *Astron. Astrophys.*, **61**, 99.
Crampton, D., Georgelin, Y. M., and Georgelin, Y. P. 1978, *Astron. Astrophys.*, **66**, 1.
Downes, A. 1983, *Monthly Notices Roy. Astron. Soc.*, **203**, 695.
Fahlman, G. G., and Gregory, P. C. 1981, *Nature*, **293**, 202.
Fahlman, G. G., Hickson, P., Richer, H. B., Gregory, P. C., and Middleditch, J. 1982, *Astrophys. J. Letters*, **261**, L1.
Felli, M., Tofani, G., Fanti, C., and Tomasi, P. 1977, *Astron. Astrophys. Suppl.*, **27**, 181.
Gregory, P. C., and Fahlman, G. G. 1980, *Nature*, **287**, 805.
Gregory, P. C., and Fahlman, G. G. 1981, *Vistas Astron.*, **25**, 119.
Haslam, C. G. T. 1974, *Astron. Astrophys. Suppl.*, **15**, 333.
Hughes, V. A., Harten, R. H., and van den Bergh, S. 1981, *Astrophys. J. Letters*, **246**, L127.
Milne, D. K. 1979, *Aust. J. Phys.*, **32**, 83.
Sedov, L. 1959, in *Similarity and Dimensional Methods in Mechanics* (Academic Press, New York), chap. 4.
Sofue, Y., and Reich, W. 1979, *Astron. Astrophys. Suppl.*, **38**, 251.

Publ. Astron. Soc. Japan **35**, 455-457 (1983)

Erratum

In der Arbeit von Kyoji NARIAI und Kazuo YOSHIOKA "Zur numerischen Rechnung der mittleren Intensitäten und Strahlungsströme in der planparallelen Sternatmosphären" [*Publ. Astron. Soc. Japan*, **35**, 113 (1983)] ließ in Tabelle 11, je für $l=1$ und 2, Spalte 2, Zeile 1,

statt $\leqq 0.06$ richtig $\leqq 0.006$,

und nur für $l=2$, Spalte 2, Zeile 2,

statt $\leqq 0.11$ richtig $\leqq 0.12$.

In der gleichen Arbeit ersetze die Tabellen 6 und 10, wegen der Verwechslung der Zeilen, mit den folgenden Tabellen.

Tabelle 6. Die Gewichte a_i und die Teilpunkte t_i für die Quadraturformel

$$\int_{1.0}^{z} f(x)K_1(x)dx = \sum_{i=1}^{4} a_i f(t_i) .$$

z	a_1	a_2	a_3	a_4	t_1	t_2	t_3	t_4
1.050	.001882	.003469	.003394	.001780	1.003442	1.016398	1.033397	1.046498
1.100	.003713	.006732	.006445	.003324	1.006825	1.032596	1.066593	1.092938
1.150	.005496	.009804	.009187	.004661	1.010152	1.048598	1.099590	1.139318
1.200	.007232	.012696	.011649	.005815	1.013424	1.064409	1.132391	1.185641
1.250	.008922	.015421	.013858	.006806	1.016642	1.080032	1.164999	1.231905
1.300	.010571	.017989	.015837	.007654	1.019809	1.095475	1.197421	1.278114
1.350	.012177	.020409	.017607	.008375	1.022925	1.110738	1.229653	1.324264
1.400	.013744	.022692	.019187	.008982	1.025991	1.125825	1.261700	1.370358
1.450	.015272	.024846	.020595	.009490	1.029009	1.140740	1.293562	1.416395
1.500	.016762	.026878	.021846	.009909	1.031981	1.155486	1.325243	1.462376
1.550	.018217	.028795	.022953	.010250	1.034906	1.170066	1.356743	1.508299
1.600	.019637	.030605	.023930	.010520	1.037787	1.184483	1.388064	1.554166
1.650	.021024	.032313	.024788	.010729	1.040625	1.198740	1.419206	1.599976
1.700	.022379	.033926	.025538	.010882	1.043419	1.212839	1.450171	1.645728
1.750	.023702	.035450	.026188	.010987	1.046172	1.226782	1.480960	1.691424
1.800	.024994	.036888	.026748	.011050	1.048884	1.240573	1.511574	1.737061
1.850	.026258	.038246	.027226	.011074	1.051556	1.254213	1.542013	1.782640
1.900	.027493	.039529	.027629	.011065	1.054189	1.267704	1.572278	1.828162
1.600	.019637	.030605	.023930	.010520	1.037787	1.184483	1.388064	1.554166
1.800	.024994	.036888	.026748	.011050	1.048884	1.240573	1.511574	1.737061
2.000	.029881	.041884	.028235	.010962	1.059341	1.294250	1.632291	1.919028
2.200	.034353	.045853	.028798	.010508	1.069208	1.345651	1.750256	2.100043
2.400	.038457	.049001	.028728	.009849	1.078532	1.394891	1.865500	2.280080
2.600	.042234	.051484	.028226	.009088	1.087352	1.442078	1.978044	2.459103
2.800	.045717	.053431	.027439	.008294	1.095702	1.487305	2.087904	2.637077
3.000	.048936	.054940	.026471	.007507	1.103615	1.530661	2.195097	2.813960
3.200	.051916	.056094	.025396	.006753	1.111118	1.572227	2.299632	2.989709
3.400	.054681	.056957	.024266	.006047	1.118238	1.612079	2.401524	3.164276
3.600	.057251	.057583	.023120	.005396	1.124998	1.650288	2.500783	3.337613
3.800	.059642	.058014	.021984	.004802	1.131420	1.686920	2.597422	3.509665
4.000	.061870	.058287	.020875	.004266	1.137523	1.722040	2.691457	3.680379
4.200	.063949	.058431	.019805	.003784	1.143326	1.755708	2.782902	3.849697
4.400	.065892	.058469	.018782	.003353	1.148846	1.787982	2.871776	4.017557
3.500	.055989	.057297	.023693	.005714	1.121661	1.631384	2.451481	3.251102
4.000	.061870	.058287	.020875	.004266	1.137523	1.722040	2.691457	3.680379
4.500	.066816	.058455	.018290	.003156	1.151505	1.803612	2.915254	4.100922
5.000	.071006	.058135	.016029	.002329	1.163857	1.876971	3.123165	4.511760
5.500	.074578	.057536	.014099	.001721	1.174788	1.942891	3.315564	4.911828
6.000	.077638	.056790	.012471	.001278	1.184472	2.002071	3.492898	5.299978
6.500	.080271	.055979	.011108	.000956	1.193057	2.055139	3.655690	5.674988
7.000	.082544	.055157	.009969	.000722	1.200672	2.102664	3.804523	6.035583
7.500	.084513	.054355	.009018	.000551	1.207423	2.145158	3.940033	6.380460
8.000	.086220	.053593	.008223	.000426	1.213406	2.183084	4.062889	6.708325
8.500	.087702	.052882	.007558	.000334	1.218703	2.216861	4.173789	7.017933
9.000	.088990	.052227	.007001	.000265	1.223385	2.246868	4.273443	7.308137
9.500	.090110	.051631	.006534	.000214	1.227515	2.273448	4.362563	7.577945
10.000	.091081	.051094	.006141	.000176	1.231148	2.296914	4.441859	7.826572
10.500	.091923	.050613	.005811	.000147	1.234334	2.317549	4.512033	8.053495
11.000	.092650	.050186	.005534	.000124	1.237118	2.335616	4.573770	8.258497
11.500	.093277	.049809	.005301	.000107	1.239538	2.351354	4.627746	8.441699
12.000	.093815	.049480	.005106	.000094	1.241632	2.364986	4.674616	8.603569
12.500	.094274	.049195	.004942	.000084	1.243433	2.376721	4.715021	8.744915
13.000	.094664	.048949	.004806	.000076	1.244972	2.386754	4.749583	8.866858

Tabelle 10. Die Gewichte a_i und die Teilpunkte t_i für die Quadraturformel

$$\int_{1.0}^{z} f(x)K_2(x)dx = \sum_{i=1}^{4} a_i f(t_i) .$$

z	a_1	a_2	a_3	a_4	t_1	t_2	t_3	t_4
1.050	.001276	.002357	.002311	.001215	1.003445	1.016410	1.033409	1.046502
1.100	.002521	.004589	.004415	.002286	1.006839	1.032642	1.066639	1.092951
1.150	.003737	.006705	.006328	.003228	1.010182	1.048699	1.099690	1.139348
1.200	.004925	.008710	.008067	.004055	1.013475	1.064584	1.132566	1.185692
1.250	.006085	.010611	.009646	.004778	1.016720	1.080297	1.165263	1.231982
1.300	.007218	.012414	.011076	.005407	1.019918	1.095849	1.197793	1.278222
1.350	.008326	.014124	.012371	.005951	1.023070	1.111233	1.230146	1.324408
1.400	.009409	.015746	.013541	.006420	1.026176	1.126456	1.262328	1.370542
1.450	.010468	.017285	.014597	.006820	1.029238	1.141519	1.294338	1.416622
1.500	.011503	.018745	.015546	.007158	1.032257	1.156425	1.326179	1.462650
1.550	.012516	.020131	.016398	.007441	1.035233	1.171176	1.357850	1.508624
1.600	.013506	.021445	.017161	.007674	1.038167	1.185774	1.389352	1.554545
1.650	.014475	.022693	.017840	.007862	1.041060	1.200220	1.420686	1.600411
1.700	.015424	.023877	.018444	.008010	1.043913	1.214518	1.451852	1.646224
1.750	.016352	.025001	.018977	.008122	1.046727	1.228668	1.482850	1.691982
1.800	.017261	.026068	.019446	.008202	1.049502	1.242673	1.513682	1.737685
1.850	.018150	.027080	.019855	.008253	1.052239	1.256534	1.544346	1.783332
1.900	.019022	.028041	.020209	.008277	1.054939	1.270254	1.574845	1.828924
1.600	.013506	.021445	.017161	.007674	1.038167	1.185774	1.389352	1.554545
1.800	.017261	.026068	.019446	.008202	1.049502	1.242673	1.513682	1.737685
2.000	.020711	.029818	.020770	.008260	1.060229	1.297273	1.635343	1.919939
2.200	.023888	.032858	.021403	.008023	1.070391	1.349677	1.754355	2.101281
2.400	.026821	.035316	.021544	.007607	1.080025	1.399982	1.870729	2.281679
2.600	.029533	.037296	.021336	.007092	1.089165	1.448277	1.984473	2.461097
2.800	.032046	.038883	.020888	.006531	1.097844	1.494642	2.095593	2.639498
3.000	.034379	.040146	.020277	.005960	1.106088	1.539155	2.204094	2.816839
3.200	.036547	.041139	.019562	.005402	1.113923	1.581889	2.309982	2.993078
3.400	.038565	.041911	.018785	.004870	1.121374	1.622911	2.413262	3.168168
3.600	.040447	.042497	.017977	.004372	1.128463	1.662288	2.513940	3.342058
3.800	.042203	.042932	.017161	.003912	1.135209	1.700082	2.612025	3.514699
4.000	.043845	.043239	.016354	.003493	1.141632	1.736352	2.707527	3.686034
4.200	.045380	.043442	.015565	.003112	1.147748	1.771156	2.800456	3.856008
4.400	.046819	.043559	.014804	.002770	1.153575	1.804548	2.890828	4.024561
3.500	.039523	.042225	.018383	.004616	1.124963	1.642801	2.463926	3.255266
4.000	.043845	.043239	.016354	.003493	1.141632	1.736352	2.707527	3.686034
4.500	.047504	.043589	.014435	.002612	1.156384	1.820731	2.935059	4.108286
5.000	.050620	.043529	.012722	.001944	1.169462	1.896774	3.146762	4.521068
5.500	.053289	.043221	.011237	.001447	1.181070	1.965234	3.342960	4.923335
6.000	.055584	.042772	.009971	.001080	1.191381	2.026800	3.524063	5.313957
6.500	.057566	.042251	.008901	.000811	1.200545	2.082096	3.690558	5.691730
7.000	.059283	.041701	.008001	.000614	1.208690	2.131689	3.842999	6.055391
7.500	.060773	.041151	.007245	.000470	1.215926	2.176097	3.981996	6.403647
8.000	.062068	.040619	.006611	.000363	1.222351	2.215786	4.108201	6.735204
8.500	.063196	.040115	.006078	.000285	1.228050	2.251182	4.222295	7.048805
9.000	.064178	.039647	.005630	.000226	1.233096	2.282673	4.324976	7.343283
9.500	.065033	.039217	.005253	.000183	1.237555	2.310607	4.416949	7.617610
10.000	.065776	.038827	.004936	.000150	1.241485	2.335305	4.498918	7.870954
10.500	.066422	.038475	.004668	.000125	1.244937	2.357059	4.571581	8.102731
11.000	.066981	.038161	.004443	.000106	1.247959	2.376136	4.635625	8.312652
11.500	.067464	.037883	.004254	.000091	1.250592	2.392783	4.691724	8.500757
12.000	.067879	.037639	.004095	.000080	1.252874	2.407231	4.740536	8.667434
12.500	.068234	.037426	.003961	.000071	1.254842	2.419693	4.782705	8.813410
13.000	.068536	.037242	.003850	.000064	1.256527	2.430369	4.818856	8.939733